# Defects and defect healing in amorphous $Si_3N_{4-x}H_y$: An *ab initio* density functional theory study

L. E. Hintzsche,[1,*] C. M. Fang,[1] M. Marsman,[1] G. Jordan,[1] M. W. P. E. Lamers,[2] A. W. Weeber,[2] and G. Kresse[1]

[1]*University of Vienna, Faculty of Physics and Center for Computational Materials Science, Sensengasse 8/12, A-1090 Vienna, Austria*

[2]*ECN Solar Energy, P.O. Box 1, 1755 ZG Petten, Netherlands*

(Received 18 February 2013; revised manuscript received 16 September 2013; published 29 October 2013)

We present an *ab initio* density functional theory study of the dominant defects in hydrogenated amorphous silicon nitrides covering different stoichiometries, the influence of hydrogen, and the influence of the annealing history. Whereas nitrogen (N) lone pair states dominate the valence band edge in stoichiometric a-$Si_3N_4$, we find that K defects, threefold coordinated silicon (Si) atoms, and Si-Si bond-related states dominate electronic defect contributions in the gap for N-deficient a-$Si_3N_{4-x}$. Hydrogen saturates the dangling Si bonds, significantly reducing the number of electronic defects related to undercoordinated Si atoms.

DOI: 10.1103/PhysRevB.88.155204 PACS number(s): 71.55.Jv, 71.15.Mb, 71.15.Pd, 71.23.Cq

## I. INTRODUCTION

Amorphous silicon (a-Si) nitrides are widely used in industry, for example, as antiwear coatings on mechanical tools as well as protective layers in the semiconductor industry. In wafer-based Si solar cells, hydrogenated a-Si nitride is also the standard antireflection and passivating layer, for both surface and bulk defects.[1,2] In general, the a-$Si_3N_{4-x}$:H layer is a compromise of optical (antireflection and absorption) properties and bulk and surface passivation. Si-rich a-$Si_3N_{4-x}$:H layers show good surface passivation quality but are highly absorbing and cannot be used for solar cell application. N-rich layers show good optical properties, but are less effective in surface passivation. For good passivation properties, a fair amount of Si-H and N-H bonds must be present in the amorphous film. These bonds connect to the amorphous network and decrease the possibility of dangling bonds. Furthermore, N-H bonds can break during the firing process and provide H atoms that might cure defects in the bulk Si layers and at the interface.[3–5]

The present study aims to determine the dominant defect class in hydrogenated Si nitride, to better understand the nature of recombination centers in Si nitride.[1,6–8] Robertson *et al.* suggested undercoordinated Si atoms (K defects, $N_3 \equiv Si$) to be the dominant defect class in the 1980s,[9] and this has subsequently been confirmed by most experiments.[6,7,10–15] According to Robertson *et al.*, K defects can be in three charge states: doubly occupied ($K^-$), singly occupied ($K^0$), or unoccupied ($K^+$).[16] However, experiments yield only indirect evidence on defects, with direct microscopic atomic-scale information mostly lacking. Moreover, only the paramagnetic $K^0$ state is detectable by electron spin resonance measurements and the tight-binding methods used by Robertson *et al.* do not meet the modern standards of *ab initio* techniques. For this reason, atomic-scale insight obtained by modern first principles simulations is highly desirable to gain a more detailed understanding of Si nitrides.

To characterize and investigate defects theoretically on the atomic scale, *ab initio* density functional theory (DFT) is nowadays indisputably the method of choice. However, defects are a minority species in the sense that most atoms maintain their preferred bonding topology. As discussed in more detail elsewhere,[17] with very few exceptions, nitrogen (N) atoms are found in a flat triangular configuration with three Si neighbors, whereas almost all Si atoms maintain the perfect fourfold coordinated tetrahedral bonding configuration in a-$Si_3N_{4-x}H_y$, regardless of the stoichiometry and hydrogen (H) content [see Fig. 1(a)]. Furthermore, for stoichiometric a-$Si_3N_4$, all Si atoms are solely surrounded by N atoms, and only when the N content decreases do homopolar Si-Si bonds form. It is then a matter of simple arithmetic to show that each Si atom will have $x$ Si and $4-x$ N neighbors in a-$Si_3N_{4-x}$, as long as the tetrahedral and triangular local coordination of Si and N, respectively, prevails. These values are indeed confirmed in our simulations and agree with the common experimental assumptions.[17]

Geometric defects and electronic states in the gap are rare; i.e, typically zero or at most one electronic defect state is observed for a supercell with 100–200 atoms. Hence, a meaningful statistical analysis cannot be drawn from a single model, and conclusions based on limited configuration sampling might be misleading. Inspection of the literature, however, shows that this "single-model" approach is often adopted to date, if the models are prepared entirely using *ab initio* DFT and cooling from the melt.[18–27] With researchers well aware of these limitations, models of amorphous structures are sometimes prepared employing force fields[28–36] or continuous random alternating networks,[37–39] but this is not entirely satisfactory either. Geometrical defects will often result in broken bonds, which are not well described by force fields, and even though the models can be reoptimized using DFT, it remains disputable whether different defect classes are properly statistically distributed in force field generated models.

Ultimately, it seems that an "all-in-one" *ab initio* DFT approach is best suited, albeit incurring significant computational costs. One purpose of the present study is to show that such calculations are possible nowadays and allow us to obtain detailed insight into a technologically relevant material.

## II. METHOD

In the present work, we use the Vienna *ab initio* simulation package (VASP),[40] the PBEsol functional,[41] and fairly soft PAW potentials for Si and N.[42,43] These soft potentials allow us to reduce the energy cutoff to about 150 eV, resulting in typically 50 plane waves per atom. We have tested these potentials for

 

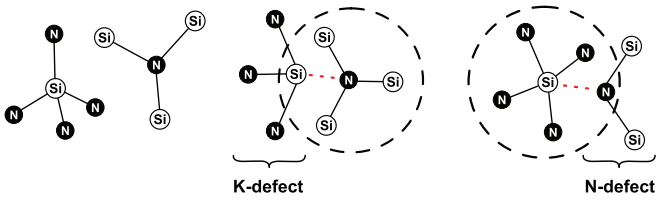


(a) ideal bonding (b) K-defect or fourfold N (c) fivefold Si or N-defect

FIG. 1. (Color online) Common geometrical bonding topologies of Si and N atoms in $Si_3N_{4-x}$. (a) Ideally coordinated Si and N atoms have four and three neighbors, respectively; (b) the K defect can be counted as either a threefold coordinated Si or a fourfold coordinated N; (c) likewise, the N defect can be counted as either a fivefold coordinated Si or a twofold coordinated N defect.

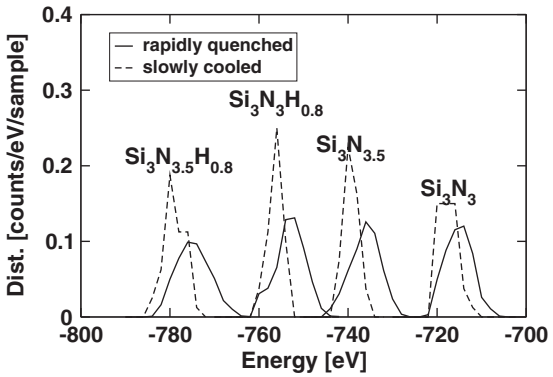


FIG. 2. Distribution of internal energy for considered ensembles. Slow annealing (dashed line) results in a significantly narrower internal energy distribution than rapid quenching (solid line).

bulk and liquid $Si_3N_{4-x}$. In comparison to accurate reference potentials, we find differences of only a few percent for the volume, band structure, phonon frequencies, and pair correlation function.[17] To allow for sufficiently long molecular dynamics simulations, we sample the electronic band structure at the Γ point and limit the models to relatively small supercells containing about 100 atoms. This is a compromise, but on the level of the pair correlation function and angular distribution function, no statistically relevant differences to 200-atom models have been found.[17]

Three stoichiometries, a-$Si_3N_4$, a-$Si_3N_{3.5}$, and a-$Si_3N_3$, are investigated, where the last two are studied with and without 12 at% H (for details see Ref. 17). The first composition is chosen, as it represents the stoichiometric form of a-Si nitride, whereas the other two represent technological relevant nitrides.

The present simulations were all performed non-spin-polarized. This is a compromise, but one that we believe corresponds well with the experimental situation. In a macroscopic sample, the Fermi level is pinned systemwide. All orbitals well below the Fermi level will be doubly occupied, whereas all well above the Fermi level will be unoccupied. This corresponds to the situation we have simulated in the present work. Singly occupied state are very rare in the present simulations, so that the neglect of spin polarization is reasonably well founded. In fact, in most of the final models, defects come in pairs with one defect level well below the Fermi level being doubly charged and the other one well above the Fermi- level being unoccupied. In a macroscopic sample, a tiny fraction of the defects close to the macroscopic Fermi level will be ultimately singly occupied, and according to our results, these defects are rare. The study of those important defects will be left for future work.

The liquid phase of the samples was generated by equilibrating for 15 ps (i.e., 10 000 time steps) at 4000 K. Then the structures were quenched rapidly to 50 K above the onset of amorphization (i.e., to 2100 K depending on the stoichiometry). At this temperature the systems were equilibrated another 15 ps. Thereafter, a 1-ns *ab initio* molecular dynamics run with a time step of 1.5 fs was performed to create a large number of amorphous model structures. For each stoichiometry, 1000 structures were generated by rapidly quenching (relaxing) every picosecond a structure into the closest local minimum. We refer to these structures as "rapidly quenched." Additionally, for each stoichiometry, 30 models were generated by slowly annealing selected structures from the long molecular dynamics run. The initial starting structures for these were taken from the long trajectory at roughly equal spacing. Then they were cooled slowly from the melt into the amorphous state by lowering the temperature by 1000 K in 75 ps. At the lowest temperature, diffusion was absent as monitored by the mean square displacement. Finally, the structures were again relaxed, and we refer to these structures as "slowly cooled."

Since all structures for a specific stoichiometry were produced by one single molecular dynamics run, they might be, to some extent, correlated. The evaluation of the statistical inefficiency[44] showed that every 40th sample of the rapidly quenched ensembles contributes completely new information to the average free energy. The 30 slowly cooled sample structures, on the other hand, can be considered independent, since we have chosen essentially uncorrelated start configurations from the long molecular dynamics run.

To gain some insight into the difference between the rapidly quenched and the slowly annealed structures, we show the distribution of the internal energy in Fig. 2. Slow annealing results in a much narrower energy distribution. However, except for a-$Si_3N_{3.5}H_{0.8}$, the slowly cooled ensembles hardly exhibit lower energy structures than the rapidly quenched ensembles (left shoulders are identical).

Figure 3 shows the pair correlation function and the angular distribution function for rapidly quenched and slowly cooled $Si_3N_{3.5}H_{0.8}$. It is well known that the structural properties of amorphous materials become more pronounced for slower cooling rates.[45] This effect has also been observed by Jarolimek *et al.* for a-Si nitride.[21] While the peaks of the pair correlation functions are slightly sharper for the slowly cooled samples, the largest differences are visible in the angular distribution function. The general structural features of a-$Si_3N_{3.5}$ are, nevertheless, almost identical for both cooling strategies, suggesting that the small ensembles are a reasonable compromise between efficiency and accuracy. We show one further test for the defect concentrations below.

An automated procedure is adopted to characterize the defect-related properties. Since we are mainly interested in the properties of electronic states in the vicinity of the band gap, our analysis considers only the three highest occupied

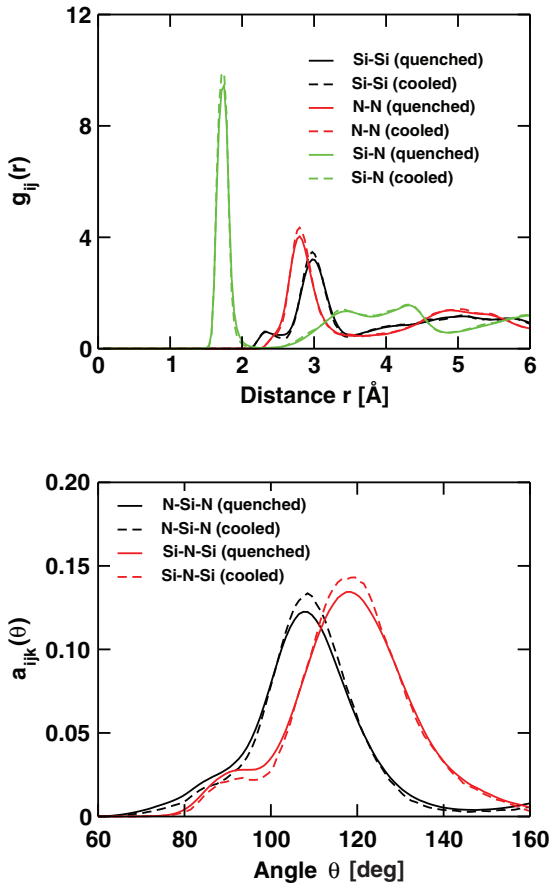


FIG. 3. (Color online) Pair correlation functions, $g_{ij}$, and angular distribution functions, $a_{ijk}$, of the rapidly quenched and slowly cooled a-$Si_3N_{3.5}H_{0.8}$ samples. Slowly cooled samples show slightly more order, with more pronounced peaks, in particular, in the angular distribution function.

and three lowest unoccupied states for each structure. We inspect whether these electronic states are strongly localized on individual N or Si atoms and whether these atoms correspond to a geometrical defect. In fact, in about 65% of the cases, the electronic defect state is strongly localized on or close to a geometrical defect. Nevertheless, in 35% of the cases, the electronic defect state is extended over several atoms showing no obvious correlation with geometric defect centers. To automatically correlate the electronic defect states with geometric defect centers, a fully automatic procedure for the determination of geometrical defects is obviously required. To this end, the position of geometrical defects in each structural model was determined by first building a nearest-neighbor list using a fairly large radial cutoff. In the second step, for overcoordinated atoms, the longest bond is removed from the list until all atoms are either ideally coordinated or undercoordinated (compare Fig. 1). In this step, overcoordinated atoms are converted into neighboring undercoordinated atoms, leaving the *total defect density* unmodified. Removing overcoordinated atoms also corresponds to the common experimental notion that the dominant defects are K defects (threefold coordinated Si atoms) and N defects (twofold coordinated N atoms), and as shown in Fig. 1 it is, at any rate, not unambiguously possible to distinguish between overcoordinated and undercoordinated geometrical defects.

## III. RESULTS

### A. Defect classification

For selected prototype defects, the charge density and the local electronic density of states (DOS) are shown in Fig. 4. For each example, the DOS is aligned with respect to the Fermi level, which is chosen to lie midgap.

In our simulations, the most common defect is the K defect, which corresponds to a threefold coordinated Si atom [see Fig. 4(a)]. The electronic defect state is a dangling $sp^3$ orbital pointing towards the missing N atom. The defect state can be

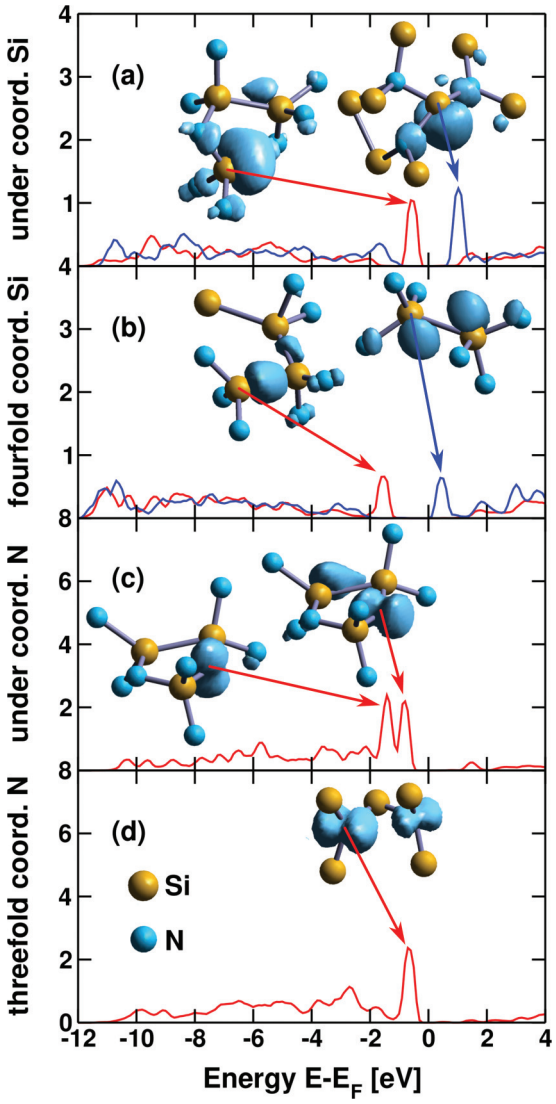


FIG. 4. (Color online) Local structure around exemplary geometrical defects and electronic density of states (DOS) evaluated at the corresponding sites (origin of arrow): (a) Si-dangling bond (K defect), (b) bonding and antibonding states on fourfold coordinated Si, (c) N lone pair and dangling bond (N defect), and (d) lone pair on threefold coordinated N. Also shown is the charge density corresponding to the peak in the DOS. The contributions to the DOS can be either occupied (red line) or unoccupied (blue line).

either occupied (red line) or unoccupied (blue line), and the Kohn-Sham eigenvalues can be located in the gap, or gradually merge into the conduction or valence band tails, or even overlap with the valence or conduction band. Only midgap defect states are well localized, whereas states that are close or in the valence or conduction band are less well localized. On average, only one of two geometrical K defects will result in an electronic defect state in the band gap, and therefore, a strict one-to-one correspondence between geometrical defects and electronic defect states in the gap does not exist.

The second class of defect states is related to Si-Si bonds or larger Si networks or Si chains. Compared to the Si-N bond, the Si-Si bond results in a much reduced bonding-antibonding splitting. If the local tetrahedral Si environment is distorted or a Si-Si bond is particularly short or long, electronic states in the band gap can be introduced. Examples of such defect states are shown in Fig. 4(b). For strong local distortions, $sp^3$ orbitals hybridize less efficiently with neighboring atoms and the charge distribution is sometimes reminiscent of K defects. Furthermore, as the N content decreases, the number of homopolar Si-Si bonds grows, and larger Si percolation networks develop.[17,21] Within such a Si network, some bonding or antibonding Si $3p$ linear combinations can move into the gap [Fig. 4(b), left]. Using an automatic procedure, Si-Si states are difficult to distinguish from other states related to a distorted Si environment, as both defect classes tend to be intermingled. Visual inspection of the charge density, however, suggests that the majority (over 70%) of the gap states that cannot be assigned to undercoordinated atoms are localized on Si-Si bonds. This observation is similar to a recent finding of Khomyakov *et al.* for a-Si.[46]

N defects, twofold coordinated N atoms, are rarely found and they are entirely absent in the slowly cooled N-deficient samples: in the nitrogen-deficient case, a surplus of Si atoms exists, and Si atoms grab any existing N-dangling bond. Although only a small number of N defects are present in the rapidly quenched ensembles, we, nevertheless, show their electronic properties in Fig. 4(c). N defects are characterized by two localized doubly occupied states close to the valence band edge. Normally, N in $Si_3N_{4-x}$ adopts a flat coordination with three Si neighbors forming $sp^2$ hybrid orbitals that develop bonding and antibonding linear combinations with the three neighboring Si atoms. The remaining two electrons form a lone nonbonding pair perpendicular to the $NSi_3$ plane. This state corresponds to the left peak. The second peak is the dangling bond state related to the broken N-Si bond. The energetic ordering of these two states depends on the local geometry and can interchange. Nevertheless, every twofold coordinated N atom is characterized by two sharp resonances in the electronic DOS, both close to the valence band maximum.

The final class of defects is distorted N centers (N-$Si_3$), shown in Fig. 4(d). A strong local distortion or unfavorable electronic environment can shift the N lone pair states up into the band gap. This is, again, a fairly rare defect species, always doubly occupied and energetically close to the valence band edge.

In summary, the dominant geometrical defects resulting in gap states are threefold coordinated Si atoms (K defects) and tetrahedrally coordinated, but distorted, Si-Si bonds or Si

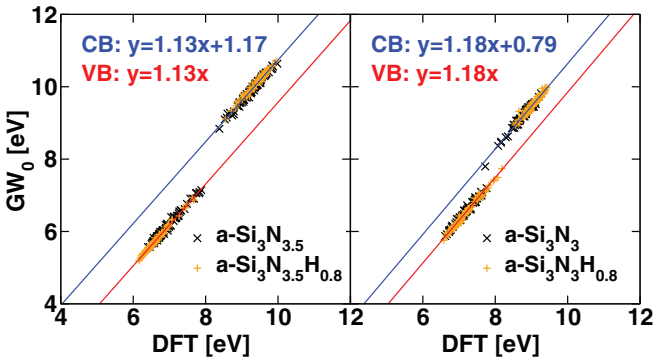


FIG. 5. (Color online) Eigenvalues of the highest occupied and lowest unoccupied orbitals for DFT and $GW_0$ calculations.[17]

percolation networks [Figs. 4(a) and 4(b)]. In our simulations the K defects are mostly doubly occupied $K^-$ (below the average Fermi level) or unoccupied $K^+$. Since the defect density decreases towards the Fermi level, only a small fraction of geometrical defects qualifies to become singly occupied, namely, those that are close to the Fermi level. Ultimately, only singly occupied K defects are easy to measure, for instance, in paramagnetic resonance experiments, and as already mentioned, the study of singly charged $K^0$ defects is left for future studies. The important question we address in the remainder of the paper is how the defect concentration changes with stoichiometry and annealing history.

### B. Energy and defect resolved density of states

In Fig. 6, we analyze the averaged defect contributions to the valance and conduction band tails. Black lines correspond to the number of states localized on undercoordinated atoms, whereas the red lines correspond to the electronic DOS on ideally coordinated atoms. To obtain more realistic quasiparticle energies ($x$ axis), we have calculated $GW_0$ corrections for about 100 selected models.[17] For $Si_3N_{3.5}H_y$ and $Si_3N_3H_y$, the corrections simply shift the unoccupied states up by $\Delta = 1.17$ eV and $\Delta = 0.79$ eV, as demonstrated in Fig. 5.

Obviously, the lowest defect density is observed in slowly cooled a-$Si_3N_{3.5}H_{0.8}$ (Fig. 6; top right panel, dashed lines), whereas the highest defect density is observed in rapidly quenched a-$Si_3N_3$ (lower left panel, solid lines). Slower cooling reduces the defect density significantly (compare left and right columns). Furthermore, increasing the N deficiency increases the defect density (compare upper and lower rows and note the different scales). This is related to an increase of the number of Si-Si bonds causing a reduced bonding-antibonding splitting, a reduction of the band gap, and a concomitant increase in the defect density. Finally, H significantly decreases the number of defect states in the gap (compare solid and dashed lines), in particular, for the slowly cooled samples.

To obtain more quantitative results on defect-related states, we have integrated the defect densities in Fig. 6 between $-1.2$ and 1.2 eV and show the results in Fig. 7. The cooling rate has a strong influence on the number of coordination defects (filled black bars compared to hatched bars), whereas it has remarkably little influence on the number of electronic

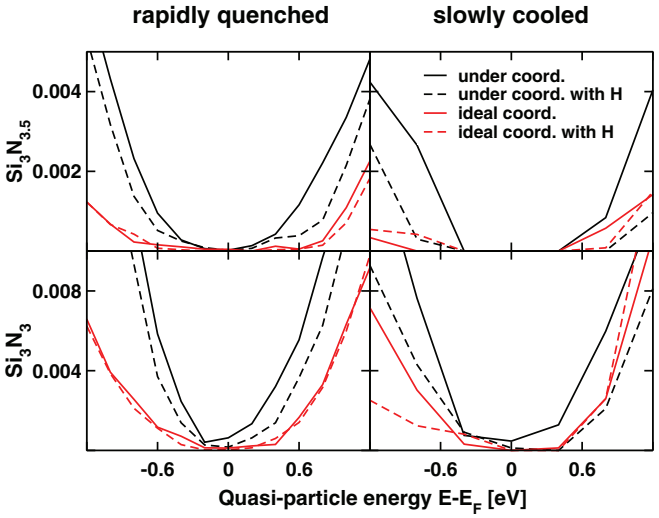


FIG. 6. (Color online) Defect density of $Si_3N_{3.5}$ and $Si_3N_3$ close to the Fermi level for rapidly quenched (left column) and slowly cooled (right column) ensembles. The total DOS is assigned to atoms with under- and ideal coordination (black and red lines). Additional H (dashed lines) reduces the number of electronic defect states originating from undercoordinated atoms.

defect states related to ideally coordinated atoms (filled red bars). Although the statistics of the slowly cooled samples is not very good, we can extract additional information on the influence of H. Hydrogen mainly cures the coordination defects, and influences the number of electronic defect states related to ideally coordinated atoms very little. This is easy to understand, as the coordination defects are mainly K defects, and H can easily attach to a K defect resulting in a $N_3 \equiv$ Si-H center.

Since size effects can be important, we have created 500 rapidly quenched models for a-$Si_3N_{3.5}$ and a-$Si_3N_{3.5}H_{0.8}$ containing twice as many atoms as the small structures considered so far. These calculations are about four times more

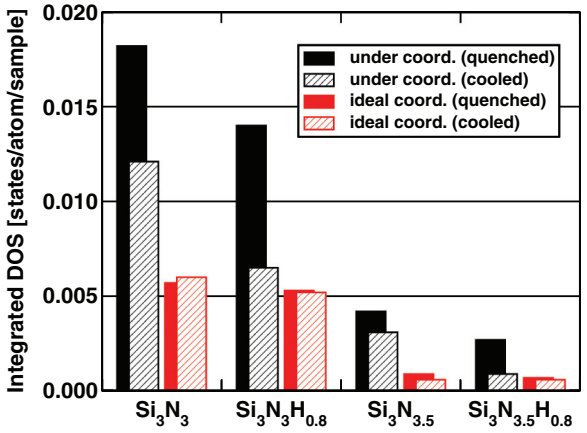


FIG. 7. (Color online) Coordination defects and ideally coordinated defects within ±1.2 eV of the Fermi level (placed midgap) for a-$Si_3N_xH_y$. Without H, the dominant defect class is undercoordinated atoms, whereas the numbers of electronic defect states related to undercoordinated and geometrically ideally coordinated atoms are about equal when H is present.

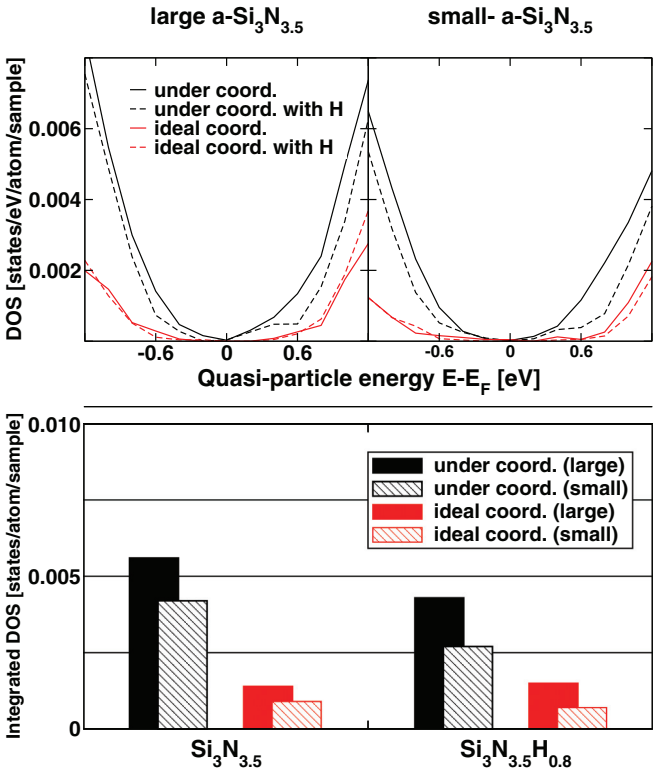


FIG. 8. (Color online) As in Figs. 6 and 7, we compare the normalized defect contributions to the total density of states of a-$Si_3N_{3.5}$, but for two system sizes. Although the larger samples show a higher defect density, the contributions from undercoordinated atoms remain dominant and H still mainly cures coordination defects.

expensive than the calculations for the smaller ensembles, and possibly not as well equilibrated. A comparison of the defect contributions between −1.2 and 1.2 eV around the Fermi level is shown in Fig. 8. We still observe that undercoordinated atoms are dominant in the rapidly quenched sample structures and that H, again, mainly passivates undercoordinated Si atoms. Despite the fact that the large samples show a higher defect density, the essential conclusions are unmodified.

## IV. DISCUSSION AND CONCLUSIONS

Our present results can be easily rationalized and are in good agreement with the present experimental evidence and prevailing assumptions. The first important observation is that defects in a-Si nitride do not posses one unique energy position in the gap, but the energy-resolved defect density rather decays from the band edges towards midgap (Fig. 6). This suggests that most geometrical defect centers will by doubly occupied, if they are located well below the macroscopic Fermi level, or unoccupied, if they are well above the macroscopic Fermi level. Only a small fraction of geometrical defects will be ultimately singly occupied and visible in, e.g., paramagnetic resonance experiments or other experiments that are sensible to singly occupied levels.

The second observation is that, in the absence of H, the occupied as well as the unoccupied defect states are clearly dominated by K defects (threefold coordinated Si

atoms) as experimentally agreed. As emphasized above, in our simulations, most of them are either doubly charged ($K^-$) or unoccupied ($K^+$). Furthermore, and somewhat unexpectedly, at least one-third of the electronic defect states are related to states localized on topologically ideally coordinated Si sites. Slower annealing and H strongly reduce the number of K defects but hardly change the number of defect states localized on ideally coordinated Si atoms. Thus topologically ideally coordinated, but distorted, Si atoms might be equally important as K defects whenever H is present. This result closely resembles the previous observations for amorphous hydrogenated Si[46] and necessitates a careful reconsideration of data for a variety of amorphous materials. One should, however, also keep in mind that H is a very mobile species. One could imagine that $N_3 \equiv$ Si-H centers, which are omnipresent in our H-rich models, are easily converted into $N_3 \equiv$ Si· ($K^0$ defects) by impinging light or thermal degradation. This is certainly an issue that warrants further studies, as well as a detailed study of the possible charge states of geometrical K defects.

Methodologically, we have demonstrated that *ab initio* techniques and today's computational recourses can be utilized effectively to sample the configuration space of amorphous structures. Since geometrical defects and electronic properties are strongly intertwined, a consistent treatment of structure generation and electronic analysis is required and attainable today.

## ACKNOWLEDGMENTS

This work is part of the HiperSol project (High Performance Solar Cells) funded by European Commission Grant No. MMP3-SL-2009-228513. Supercomputing time on the Vienna Scientific Cluster (VSC) is gratefully acknowledged.

*Corresponding author: leif.eric.hintzsche@univie.ac.at

[1] A. G. Aberle, Prog. Photovolt. Res. Appl. **8**, 473 (2000).
[2] F. Duerinckx and J. Szlufcik, Solar Energy Mater. Solar Cells **72**, 231 (2002).
[3] C. Boehme and G. Lucovsky, J. Vac. Sci. Technol. A: Vacuum Surf. Films **19**, 2622 (2001).
[4] J. Hong, W. M. M. Kessels, F. J. H. van Assche, H. C. Rieffe, W. J. Soppe, A. W. Weeber, and M. C. M. van de Sanden, Prog. Photovolt. Res. Appl. **11**, 125 (2003).
[5] M. W. P. E. Lamers, K. T. Butler, P. E. Vullum, J. H. Harding, and A. Weeber, Phys. Status Solidi A **210**, 658 (2013).
[6] P. M. Lenahan and S. E. Curry, Appl. Phys. Lett. **56**, 157 (1990).
[7] W. L. Warren, P. M. Lenahan, and S. E. Curry, Phys. Rev. Lett. **65**, 207 (1990).
[8] J. Singh and K. Shimakawa, *Advances in Amorphous Semiconductors* (CRC Press, London, 2003).
[9] J. Robertson and M. J. Powell, Appl. Phys. Lett. **44**, 415 (1984).
[10] D. T. Krick, P. M. Lenahan, and J. Kanicki, J. Appl. Phys. **64**, 3558 (1988).
[11] D. T. Krick, P. M. Lenahan, and J. Kanicki, Phys. Rev. B **38**, 8226 (1988).
[12] W. L. Warren and P. M. Lenahan, Phys. Rev. B **42**, 1773 (1990).
[13] W. L. Warren, F. C. Rong, E. H. Poindexter, G. J. Gerardi, and J. Kanicki, J. Appl. Phys. **70**, 346 (1991).
[14] L. Zhong and F. Shimura, Appl. Phys. Lett. **62**, 615 (1993).
[15] D. Q. Chen, J. M. Viner, and P. C. Taylor, Solid State Commun. **98**, 745 (1996).
[16] J. Robertson, W. L. Warren, and J. Kanicki, J. Non-Crystal. Solids **187**, 297 (1995).
[17] L. E. Hintzsche, C. M. Fang, T. Watts, M. Marsman, G. Jordan, M. W. P. E. Lamers, A. W. Weeber, and G. Kresse, Phys. Rev. B **86**, 235204 (2012).
[18] F. Alvarez and A. A. Valladares, Phys. Rev. B **68**, 205203 (2003).
[19] L. Giacomazzi and P. Umari, Phys. Rev. B **80**, 144201 (2009).
[20] V. A. Gritsenko, S. S. Nekrashevich, V. V. Vasilev, and A. V. Shaposhnikov, Microelectron. Eng. **86**, 1866 (2009).
[21] K. Jarolimek, R. A. de Groot, G. A. de Wijs, and M. Zeman, Phys. Rev. B **82**, 205201 (2010).
[22] S. S. Nekrashevich, A. V. Shaposhnikov, and V. A. Gritsenko, JETP Lett. **94**, 202 (2011).
[23] A. Pasquarello, M. S. Hybertsen, and R. Car, Nature **396**, 58 (1998).
[24] J. Sarnthein, A. Pasquarello, and R. Car, Phys. Rev. Lett. **74**, 4682 (1995).
[25] A. Pasquarello and R. Car, Phys. Rev. Lett. **80**, 5145 (1998).
[26] A. Pasquarello, M. S. Hybertsen, and R. Car, Phys. Rev. Lett. **74**, 1024 (1995).
[27] M. Boero, A. Pasquarello, J. Sarnthein, and R. Car, Phys. Rev. Lett. **78**, 887 (1997).
[28] N. Umesaki, N. Hirosaki, and K. Hirao, J. Non-Crystal. Solids **150**, 120 (1992).
[29] L. Ouyang and W. Y. Ching, Phys. Rev. B **54**, R15594 (1996).
[30] F. De Brito Mota, J. F. Justo, and A. Fazzio, Int. J. Quantum Chem. **70**, 973 (1998).
[31] F. de Brito Mota, J. F. Justo, and A. Fazzio, J. Appl. Phys. **86**, 1843 (1999).
[32] S. Mukhopadhyay, P. V. Sushko, A. M. Stoneham, and A. L. Shluger, Phys. Rev. B **70**, 195203 (2004).
[33] L. Giordano, P. V. Sushko, G. Pacchioni, and A. L. Shluger, Phys. Rev. Lett. **99**, 136801 (2007).
[34] M. Ippolito and S. Meloni, Phys. Rev. B **83**, 165209 (2011).
[35] K. T. Butler, M. P. W. E. Lamers, A. W. Weeber, and J. H. Harding, J. Appl. Phys. **110**, 124905 (2011).
[36] R. P. Vedula, N. L. Anderson, and A. Strachan, Phys. Rev. B **85**, 205209 (2012).
[37] P. Kroll, J. Non-Crystal. Solids **293**, 238 (2001).
[38] S. Y. Lin, Opt. Mater. **23**, 93 (2003).
[39] S. Z. Karazhanov, P. Kroll, A. Holt, A. Bentzen, and A. Ulyashin, J. Appl. Phys. **106**, 053717 (2009).
[40] G. Kresse and J. Furthmüller, Phys. Rev. B **54**, 11169 (1996).
[41] J. P. Perdew, A. Ruzsinszky, G. I. Csonka, O. A. Vydrov, G. E. Scuseria, L. A. Constantin, X. Zhou, and K. Burke, Phys. Rev. Lett. **100**, 136406 (2008).
[42] P. E. Blöchl, Phys. Rev. B **50**, 17953 (1994).
[43] J. Furthmüller, J. Hafner, and G. Kresse, Phys. Rev. B **50**, 15606 (1994).
[44] M. P. Allen and D. J. Tildesley, *Computer Simulation of Liquids* (Oxford University Press, New York, 1989).
[45] K. Vollmayr, W. Kob, and K. Binder, Phys. Rev. B **54**, 15808 (1996).
[46] P. A. Khomyakov, W. Andreoni, N. D. Afify, and A. Curioni, Phys. Rev. Lett. **107**, 255502 (2011).